# RF MEMS for Ubiquitous Wireless Connectivity:

## Part 1—Fabrication

*Héctor J. De Los Santos, Georg Fischer, Harrie A.C. Tilmans, and Joost T.M. van Beek*

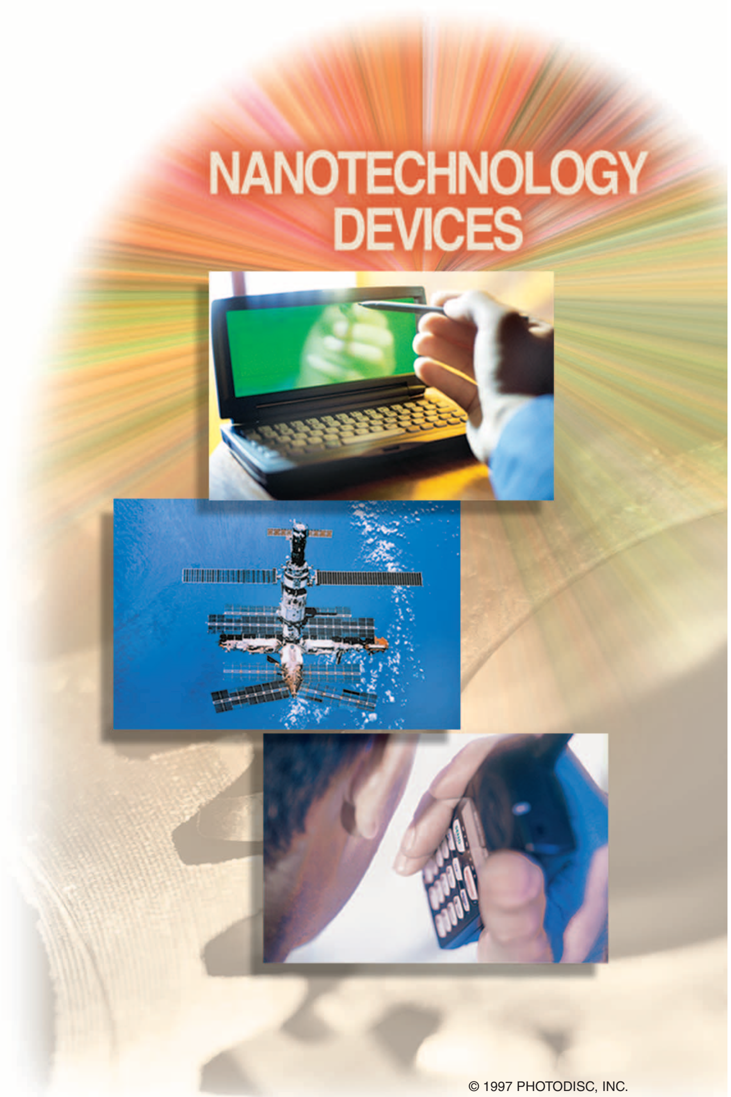




The application of microelectromechanical systems (MEMS) technology to radio-frequency (RF)/ microwave systems is on the verge of revolutionizing wireless communications [1]. Indeed, the fact that RF MEMS enables superior passive devices, such as switches, switchable (two-state) capacitors, tunable capacitors (varactors), inductors, transmission lines and resonators, makes it a prime candidate to enable a plethora of wireless appliances operating in the home/ground, mobile, and space spheres [2], such as handsets, base stations, and satellites. The quintessential properties with which these systems are endowed are those of low power consumption and reconfigurablity. It is for these reasons that RF MEMS is believed to be a key technology to enable ubiquitous wireless connectivity. In this context, it is the aim of this article to expose the impact and status of the application of RF-MEMS switchable capacitors, varactors, and switches in the three elements of this paradigm, namely, handsets, base stations, and satellites. In particular, issues such as system-level motivation/justification for RF MEMS, device requirements, high-volume manufacturing, packaging, and state-of-the-art performance and reliability, are presented.

Part One of this article focuses on fabrication (surface and bulk micromachining) techniques and their

*Héctor J. De Los Santos (NanoMEMSLLC@aol.com) is with NanoMEMS Research, LLC Irvine, CA 92604 USA. Georg Fischer is with Lucent-Bell Labs Europe Nuremberg, Germany. Harrie A.C. Tilmans is with Inter-University Microelectronics Center (IMEC) Leuven, Belgium. Joost T.M. van Beek is with Philips Research Laboratories Eindhoven, The Netherlands.*

 1527-3342/04/$20.00©2004 IEEE 

limitations, comparing key physical actuation mechanisms upon which RF-MEMS devices may be predicated and on device-level packaging. Part Two, directly following this article, focuses on the progress and impact of RF-MEMS devices on wireless systems, in particular, on handsets, base stations, and space applications.

## Fundamentals of RF-MEMS Technology

### *Fabrication*

RF-MEMS fabrication technology builds upon the well-established discipline of integrated circuit (IC) fabrication. In fact, it may be understood with reference to the conventional two-dimensional (2-D) IC fabrication process [1], Figure 1, which is based on photolithography and chemical etching and predicated upon the following fundamental steps.

1) The wafer is coated with a barrier (typically $SiO_2$ for a silicon wafer).
2) The surface is coated with a polymeric light-sensitive material, called photoresist (PR).
3) A photomask, a square glass plate with a patterned emulsion or metal film on one side, is placed over the wafer and the PR is exposed through the mask to high-intensity, ultraviolet (UV) light wherever the mask is transparent.

The PR is developed by means of a process similar to that for developing photographic film and may be either positive or negative, resulting in the following respective outcomes.

1) When UV light strikes the positive PR, it weakens the polymer so that when the image is developed, the UV-exposed PR is washed, thus transferring the positive image of the mask to the resist layer.
2) When UV light strikes the negative PR, it strengthens the polymer so that when the image is developed, the resist that was not exposed to the UV light is washed away, thus transferring the negative image of the mask to the resist layer.

RF MEMS is predicated upon two main techniques to shape the third dimension, namely, *surface micromachining* and *bulk micromachining*.

In *surface micromachining*, Figure 2(a), thin-film materials are selectively added to and removed from the wafer. The film materials that are eventually removed are called sacrificial materials, wheareas those that remain are called structural materials. For example, a cantilever beam may be created on a silicon wafer by depositing $SiO_2$ as the sacrificial layer, depositing polysilicon as the structural layer, defining the beam pattern on the polysilicon layer, and finally dissolving the sacrificial layer underneath it. This last step is called *release* since it aims at rendering movable free-standing mechanical structures. Typical materials employed in surface micromachining are shown in Table 1 [3].

When a wet etchant is utilized to dissolve the sacrificial layer, however, it must be ensured that the spring

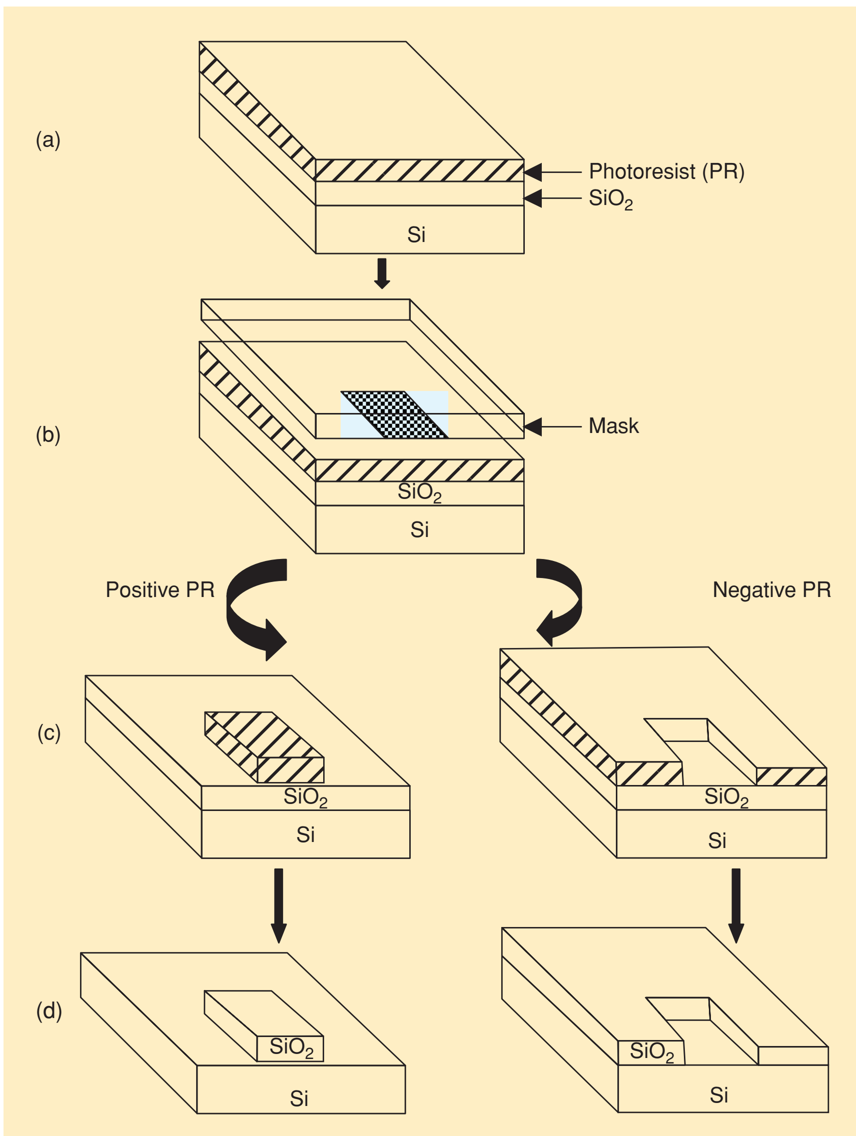


**Figure 1.** *Sketch of IC fabrication sequence.*

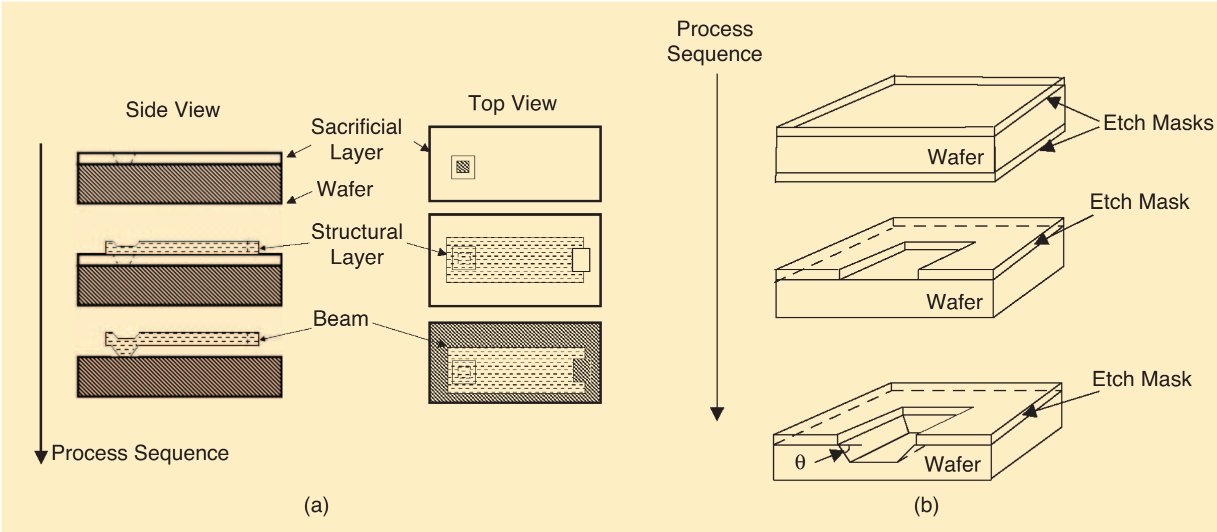


**Figure 2.** *(a) Surface micromachined beam. (b) Bulk micromachined cavity.*

**Table 1. Structural/sacrificial/etchant material systems [3].**

| Structural Material | Sacrificial Material | Etchant |
|---|---|---|
| Aluminum | Single-crystal silicon | EDP, TMAH, XeF2 |
| Aluminum | Photoresist | Oxygen plasma |
| Copper or Nickel | Chrome | HF |
| Polyimide | Aluminum | Al etch (phosphoric, acetic, nitric acid) |
| Polysilicon | Silicon dioxide | HF |
| Photoresist | Aluminum | Al etch (phosphoric, acetic, nitric acid) |
| Silicon dioxide | Polysilicon | XeF2 |
| Silicon nitride or Boron-doped polysilicon | Undoped polysilicon | KOH or TMAH |

forces of the mechanical structures overcome the wet etchant's surface tension forces. Otherwise, release will not occur properly, and the structures will end up stuck to the substrate or nearby structures. This sticking phenomenon, or stiction, may also occur during the operation of electrostatically actuated devices, in which case it may be the result of *pull-in*, discussed below [1], [3]–[5].

In *bulk micromachining*, mechanical structures are created within the confines of the wafer, Figure 2(b), by selectively removing wafer material by wet and dry etching techniques, thus exploiting the anisotropic etching rates of the different crystal planes in the wafer.

The application of MEMS in the context of integrated systems is rather appealing because by integrating three-dimensional (3-D) *freely moveable* mechanical structures in the same wafer with the electronics, it becomes possible to produce highly functional systems with novel performance levels not achievable otherwise, in particular, as it pertains to system size and weight, power consumption, and cost. The 3-D MEM structures in question, may be activated via a variety of actuation mechanisms, such as those derived from electrostatic, electrothermal, piezoelectric, electromagnetic, and electrodynamic forces. However, at the core, from a system-level or functional point of view, and irrespective of the actuation mechanism invoked, they contain two pairs of electrodes, namely, one pair via which a dc bias is applied to effect the motion, and one pair, the switching electrodes or contacts, across which the RF signal being acted upon exists. When the two pairs are insulated from one another, the configuration is referred to as a *relay*. On the other hand, if the dc and RF signal share the same control lines, the configuration is referred to as a *switch*. From a circuit point of view, relays may be classified as four-terminal devices and switches as two-terminal devices. However, it is possible, when the bias and RF sets of terminals share a common ground, to have a three-terminal relay.

From a circuit-design perspective, the nature of the device structure, namely, whether a relay or a switch, is very important. This is so because, whereas a relay possesses an intrinsic isolation between bias and RF terminals, a switch does not. Therefore, when a switch configuration is employed, a manner of decoupling bias from RF signals, e.g., a bias tee, must be used. These concepts may be visualized by examining fundamental structures for RF-MEMS relays and switches shown in Figure 3.

In this article, we focus on the progress and impact of three types of surface-micromachined RF-MEMS devices on wireless systems, namely, switchable capacitors (SC), varactors (variable/tunable capacitors), and ohmic switches. Next, a comparison among the various actuation mechanisms exploited in RF-MEMS devices is presented.

### Actuation

RF-MEMS devices, like switches, tunable capacitors and mechanical resonators, contain movable members that are set into motion via a microactuator. An RF-MEMS switching device, for instance, has just two stable states, like semiconductor RF switches. Switching between the two states is achieved through the mechanical displacement of a freely movable structural member, namely, the armature. The displacement is induced via a micro-actuator for which various actuation mechanisms exist, including *electrostatic*, *electrothermal*, *piezoelectric* and *electromagnetic* actuation [6]. The principle of operation of these four mechanisms is depicted in Figures 4, 6, 7, and 8, respectively, and illustrated for a flexural cantilever-type RF-MEMS switching device. The following subsections further discuss each actuation mechanism.

The majority of RF-MEMS devices rely on *electrostatic* actuation [7], [8], illustrated in Figure 4(a) for an RF-MEMS switching device. Electrostatic actuation is based on the attractive Coulomb force $F_{el}$ existing between charges of opposite polarity. The electrostatic attractive force of two parallel plates across which a voltage $V$ is applied is given by:

$$F_{el} = \frac{1}{2}\frac{Q^2}{\varepsilon_0 A} = \frac{1}{2}\frac{\varepsilon_0 A V^2}{d^2}, \qquad (1)$$

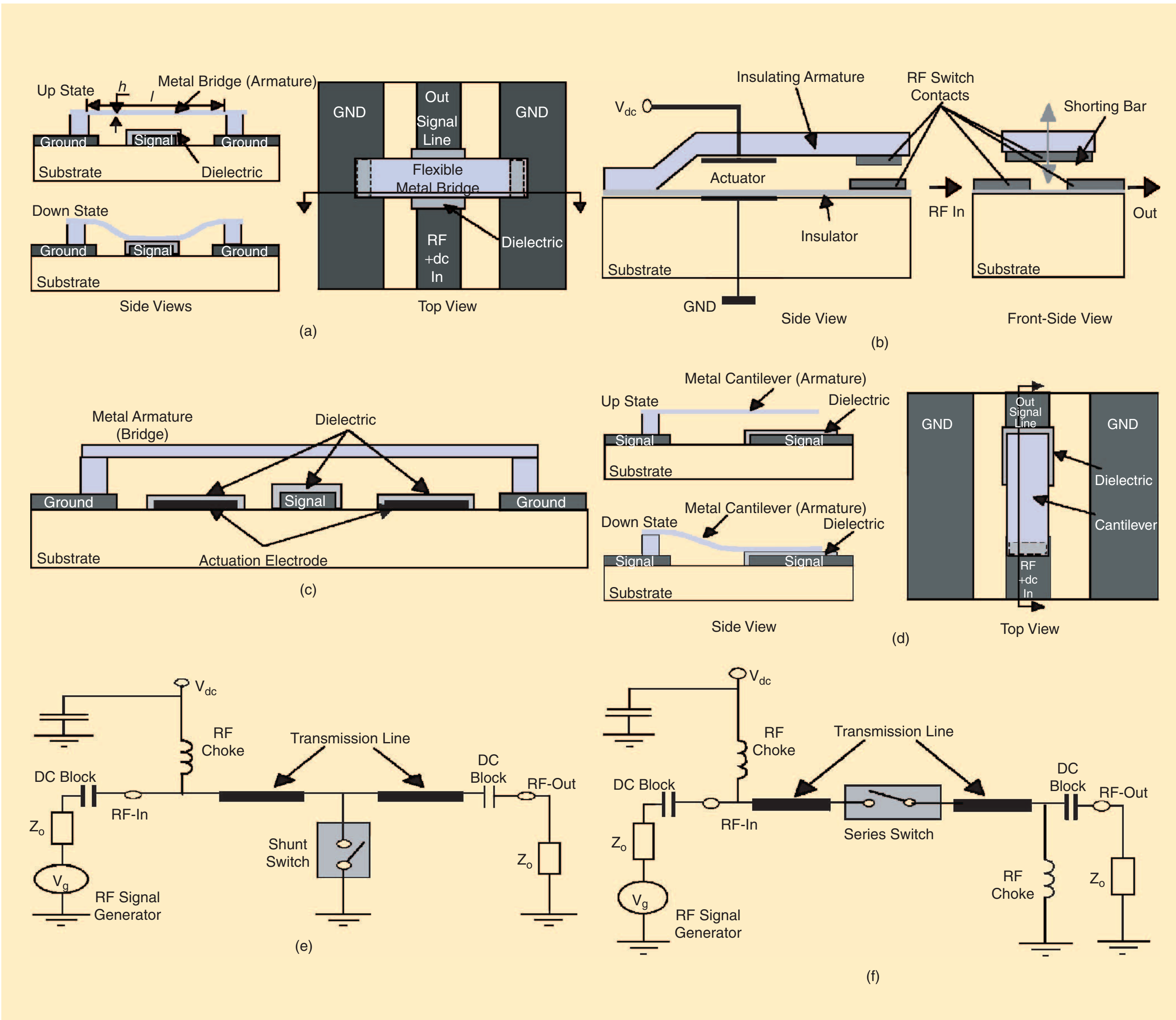


**Figure 3.** *Configuration and biasing of RF-MEMS relay and switch structures. (a) Electristatically actuated capacitive shunt switch (broadside configuration) implemented on a CPW transmission line. (b) Electrostatically actuated ohmic series relay implemented with a cantilever beam armature (broadside configuration). (c) Electrostatically actuated three-terminal capacitive shunt switch (in a broadside configuration). (d) Electrostatically actuated capacitive series switch implemented on a CPW transmision line (inline configuration). (e) Biasing network of shunt switch. (f) Biasing network of series switch.*

where $Q(= CV$, with $C = \varepsilon_0 A/d$ the capacitance) is the charge on the capacitor plates, $A$ is the plate area, $d$ is the gap spacing, and $\varepsilon_0$ is the permittivity of free space. The force is inversely proportional to the square of the gap spacing, as shown in (1). This nonlinear relationship causes instability to occur when the voltage exceeds the so-called *pull-in* (or snap-down) voltage $V_{PI}$. In other words, pull-in denotes the voltage at which control of an electrostatically actuated device, e.g., a beam, is lost due to the loss of equilibrium between electrostatic and spring forces. This phenomenon becomes apparent from an examination of the equation of equilibrium between spring and electrostatic forces whose solution gives the displacement of the movable plate of a parallel-plate capacitor, $x(V)$, Figure 4(b).

This equation is given by

$$\left(kx - \frac{\varepsilon_0 A V^2}{2\,(d_0 - x)^2}\right) = 0, \qquad (2)$$

and it implies that, starting at $V = 0^+$, $x$ will adjust itself so that (2) is *eventually* satisfied. For this adjustment in $x$ to occur, the magnitude of $V$ must be such that the *initial* value of (2) is greater than zero. In that case (2) has positive real (physical) roots, $x(V) > 0$. The voltage that demarcates this regime is that at which the difference between spring and electrostatic forces, embodied by (2) is a minimum. Its value may be found by calculating the derivative of (2) and equating it to zero, i.e.,

$$k - \frac{\varepsilon_0 A V^2}{(d_0 - x)^3} = 0. \qquad (3)$$

By simultaneously solving (2) and (3), one obtains

$$V_{PI} = \sqrt{\frac{8kd_0^3}{27\varepsilon_0 A}} \qquad \left(d_0 >> \frac{d_\varepsilon}{\varepsilon_r}\right) \qquad (4a)$$

and

$$x_{PI} = \frac{d_0}{3}, \qquad (4b)$$

where $V_{PI}$ denotes the pull-in voltage and $x_{PI}$ the displacement at which pull-in ocurrs. Figure 4(c) shows a

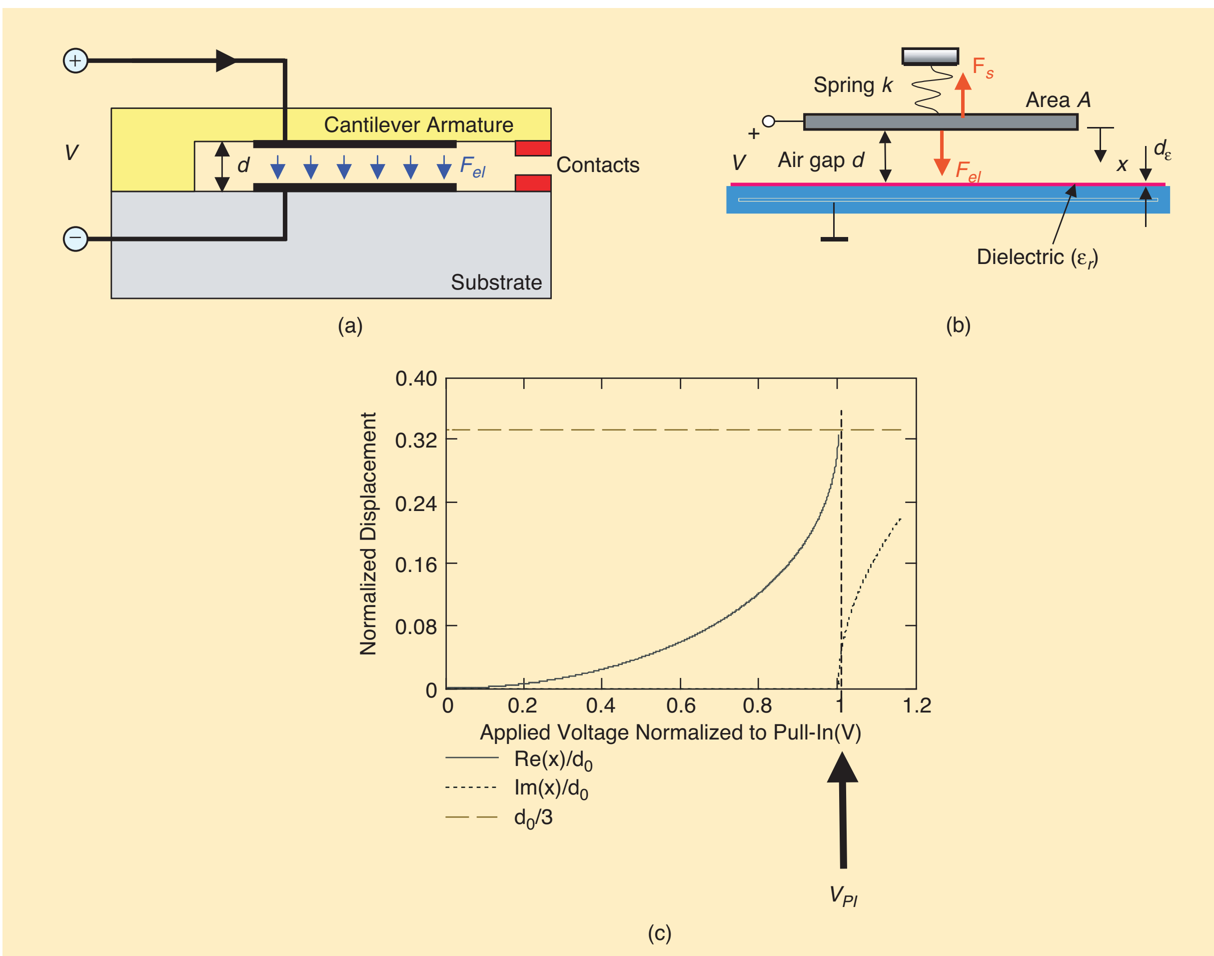


**Figure 4.** *(a) Electrostatic actuation mechanism illustrated on a microrelay. (b) Force diagram illustrated for a lumped model of an electrostatic actuator. (c) Normalized displacement versus applied voltage normalized to pull-in voltage [3].*

plot of the normalized displacement versus the applied voltage normalized to the pull-in voltage, indicating that, at pull-in, the displacement becomes imaginary, and the slope of the applied voltage no longer controls the displacement.

In lowering the voltage after pull-in has occurred, the beam releases at a (much) lower voltage called the pull-out voltage $V_{PO}$. As such, the electrostatic actuator displays a hysteresis. The pull-out voltage is approximately given by

$$V_{PO} = \sqrt{\frac{2kd_o d_\varepsilon^2}{\varepsilon_r^2 \varepsilon_0 A}} \qquad \left(d_0 >> \frac{d_\varepsilon}{\varepsilon_r}\right), \qquad (5)$$

where $\varepsilon_r$ and $d_\varepsilon$ denote the thickness and permittivity of the dielectric covering the lower electrode, respectively. In case there is no dielectric, $\varepsilon_r = 1$ and $d_\varepsilon$ must be replace by $d_R$, and $d_0$ by $(d_0 - d_R)$, where $d_R$ denotes the rest gap after closing. The expressions for the pull-in and pull-out voltages are exact for a lumped spring-mass system. For a typical RF-MEMS switch design, for which $d_o = 2.5\ \mu$m, $d_\varepsilon = 0.2\ \mu$m, $\varepsilon_r = 7$, $k = 10$ N/m, and $A = 100 \times 100\ \mu\text{m}^2$, it follows, that $V_{PI} \approx 23$ V and $V_{PO} \approx 0.7$ V.

It is pointed out that the electrostatic force $F_{el}$ will not increase indefinitely with increasing voltage but is limited by breakdown of the air gap. The breakdown field of micron-sized gaps is $\sim 3 \cdot 10^8$ V/m, leading to a maximum force of $\sim$4 mN for an electrode area of $100 \times 100\ \mu\text{m}^2$. To achieve the breakdown field across a gap of 1 $\mu$m, a rather high voltage of 300 V is required. More practical voltage levels of around 10 V result in a force of $\sim$0.004 mN, i.e., three orders of magnitude smaller than the maximum force. As microrelays equipped with low quality Au contacts already require contact forces of at least 50–100 $\mu$N in order to attain a stable and low contact resistance, electrostatic actuation is considered not very attractive unless the actuation area is chosen to be very large ($>1 \times 1\ \text{mm}^2$) and/or high actuation voltages ($>$100 V) are allowed.

The importance of pull-in cannot be overemphasized, as it poses performance limitations for a parallel-plate type tunable capacitor. As pull-in occurs at 1/3 of the gap spacing, the tuning range is limited to 150% (corrresponding to a maximum capacitance ratio of 2:1). A number of schemes to avoid pull-in have been advanced. In particular, the use of separate control and signal electrodes (so-called dual-gap approach) with respective electrode-to-top-plate separations $d_2$ and $d_1$ obeying the relationship $d_1 \leq d_2/3$, Figure 5, has resulted in the tuning range (TR) being extended from the theoretical pull-in-limited value of 50% to more than 400% [4]. A more recent implementation of the dual-gap varactor by Rijks et al., demonstrated a TR of 1,600% [5].

An electrostatic drive offers extremely low power consumption, in which power is consumed only during (switching) motion (compared to a digital inverter stage). Other advantages of using electrostatic actuation are the relatively simple fabrication technology, the high degree of compatibility with a standard IC process line, the ease of integration with planar and microstrip transmission lines, and the fast response (in the microsecond range). The main drawback of electrostatic actuation is the high actuation voltage (in the range 12–60 V) associated with the large-gap actuator required in RF-MEMS switches. Here it is difficult to combine a low actuation voltage with a good isolation of a series-configured switch (or, alternatively, a good insertion loss for a shunt-configured switch) and a robust device that is strongly resistant to shocks and vibrations. For high frequency (>100 MHz) mechanical resonators on the other hand, narrow actuation gaps are needed to attain a high electromechanical coupling factor or, equally, a small motional resistance. Note though that high-frequency mechanical resonators are very stiff, which in turn implies a high bias voltage for achieving a high coupling factor. Clearly, a compromise in the design must be made. In case the available supply voltage is limited, e.g., to 3–5 V as in handheld phones, on-chip, high-voltage generators, such as the Dickson-type dc voltage multiplier circuit, may be

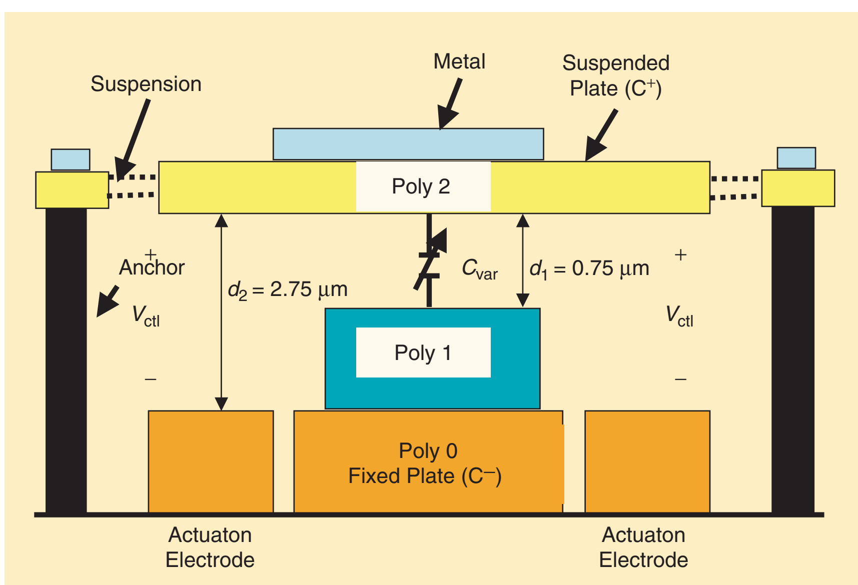


**Figure 5.** *Cross-sectional view of MEMS varactor [4]. $V_{ctl}$ denotes the actuation or control voltage.*

incorporated. This is either done monolithically, e.g., through "above-IC processing," or in a hybrid fashion, as has recently been demonstrated by Motorola [10].

*Piezoelectric actuation* and *detection* are based on the inverse piezoelectric effect and the direct piezoelectric effect, respectively [11]. A piezoelectric material provides its own *internal* bias, either due to the absence of a center of symmetry in single-crystal materials [e.g., aluminum nitride (AlN) or zinc oxide (ZnO)] or to a permanent polarization in the case of ferroelectric materials, e.g., ferroelectrics of the lead zirconate titanate (PZT) family. The inverse piezoelectric effect is manifested as a mechanical deformation in the material if subjected to an electric field. Upon applying a voltage $V$, the piezoelectric layer, which is fixed on top of a cantilever beam as in Figure 6, an equivalent bending moment $M_{PE}$ at the tip will be induced. The bending moment causes the cantilever to bend with a tip deflection $\delta = M_{PE}\, l^2/2EI$, where $EI$ is the equivalent bending stiffness of the beam and $l$ is the beam length. For the case where the piezolayer is much thinner than the carrier layer and the mechanical effect of the electrodes is ignored, a simple expression for the piezoelectric bending moment can be expressed as follows [12]:

$$M_{PE} \approx \tfrac{1}{2} d_{31} E p b h_s V \quad (h_p << h_s), \tag{6}$$

where $d_{31}$ is the piezoelectric coefficient of the piezolayer, $E_p$ is the Young's modulus of the piezolayer, $b$ is the beam width, and $h_s$ and $h_p$ are the thickness of the carrier layer and piezolayer, respectively. The above expression indicates that materials with a high piezoelectric coefficient are advantageous for use in piezoelectric actuators. Typical values for piezoelectric coefficient $d_{31}$ vary from ~3 pC/N for AlN, ~5 pC/N for ZnO, and ~100 pC/N for PZT materials. As opposed to electrostatic actuation, piezoelectric actuation does not display mechanical instability, i.e., pull-in or snap-down does not occur in a piezoelectric actuator. On the contrary, the actuator closes in a linear fashion. The threshold voltage needed to close the gap, i.e., tip deflection equals the gap spacing ($\delta = d_o$), is approximately given by

$$V_{Th} \approx \tfrac{1}{3} \frac{1}{d_{31}} \left(\frac{h_s}{l}\right)^2 \frac{E_s}{E_p} d_o \quad (h_p << h_s), \tag{7}$$

whereby (6) is used for the bending moment, and a prismatic beam with rectangular cross section ($b \times h_s$, where $b$ denotes the beam width) is assumed. For an actuator using AlN as the piezoelectric material ($E_{p,\mathrm{AlN}} = 320$ GPa), aluminum as the carrier layer ($E_{s,Al} = 70$ GPa), a gap spacing $d_o = 2.5\ \mu$m, and a ratio $h_s/l = 0.01$, the threshold voltage to close is approximately 6 V. Replacing AlN with PZT ($E_{p,\mathrm{PZT}} = 70$ GPa), the threshold voltage drops to below 1 V. In other words, low-voltage actuation in combination with large air gaps is feasible, in particular when using piezoelectric materials with a high piezoelectric coefficient. Using standard mechanics, an expression for the contact force $F_c\,(= 3\, M_{PE}/2l - 3\, \mathrm{d_o} EI/l^3)$ can be derived. For the example above, the achievable contact force for an AlN-based actuator is around 3 $\mu$N for a voltage of 15 V assuming a beam width $b = 50\ \mu$m. For a PZT-based actuator with the same dimensions, the contact force is close to 10 $\mu$N for an applied voltage of 5 V.

Piezoelectric actuators, in general, display a fast response with reasonable power consumption, but the main drawback is the complex technology. The latter is the main reason why piezoelectric actuation is not so much used. Only a few examples are known of piezoelectrically driven switching devices [13], tunable capacitors [14], and mechanical resonators [15].

*Electrothermal actuation* is based on the thermal expansion, due to a temperature elevation, as a result of heat generation by an electrical current $I$ in a resistor [16], [17]. If the resistor $R$ is located in the upper fibers of the beam, as in Figure 7, a thermal wave propagating and attenuating in the thickness direction results. This, in turn, creates a bending moment $M_{Th}$, which is used to actuate the beam. A crude approximation of the thermal bending moment for the cantilever actuator of Figure 7 is given by [17]:

$$M_{Th} \approx \frac{\alpha h^3 E_Y}{3\lambda l} I^2 R, \tag{8}$$

where $\alpha$ is the coefficient of thermal expansion of the

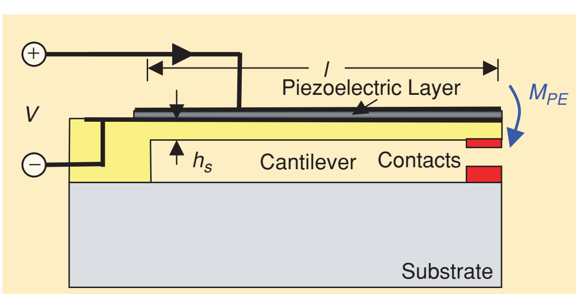


**Figure 6.** *Piezoelectric actuation mechanism illustrated on a microrelay.*

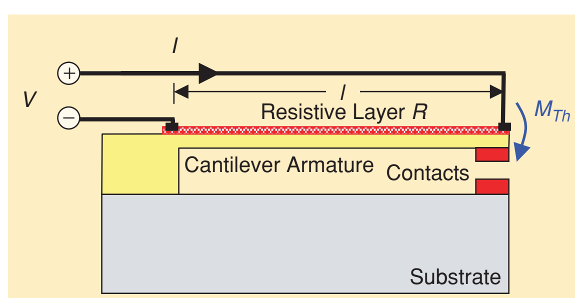


**Figure 7.** *Electrothermal actuation mechanism illustrated on a microrelay.*

beam material, $l$ is the beam length, $E_Y$ is the Young's modulus of the beam material, $\lambda$ is the thermal conductivity of the beam material, and $I^2R$ denotes the power dissipated in the resistor. Also, just as in the piezoelectric actuator, pull-in or snap-down does not occur here.

In a mechanical resonator, to avoid frequency doubling, a dc bias voltage or current is superimposed onto the ac drive signal. Due to the irreversible conversion of electric energy into heat in the thermal transducer, detection of the motion must be accomplished through other means. Possible means that can be combined with electrothermal actuation are capacitive detection or piezoresistive detection [6].

Advantages of electrothermal actuation are the low actuation voltage and the very simple built-up and associated simple process flow. Drawbacks are the slow response (hundreds of microseconds) and the high power consumption (heat dissipation and continuous current drain in the actuated state). This is the reason why relatively few examples exist of thermally actuated switches, tunable capacitors, or resonators. To avoid continuous power consumption (current drain) of the switch in the down-state, other means, like electrostatic clamping, can be implemented as demonstrated in the switch developed by LETI [18].

The *electromagnetic actuator* (also called the *variable reluctance* actuator), depicted in Figure 8, forms the dual analog of the electrostatic actuator. The actuator shown consists of a yoke, the movable beam, and a driving coil with an excitation winding of $N$ turns. A current $I$ in the coil sets up a magnetic flux $\Phi$ in the yoke and the gap. The yoke and part of the beam (or the entire beam) consist of a highly permeable material ($\mu_r \rightarrow \infty$), and are separated by a gap, usually filled with air. Together, they define a magnetic circuit through which the magnetic flux $\Phi$ flows. The total reluctance, defined as the ratio of the magnetomotive force (MMF) $NI$ and the flux passing through the magnetic circuit, is approximately equal to the reluctance $R_m$ of the air gap, given by $R_m = d/\mu_0 A$. Hence, the magnitude of the flux is controlled by the gap spacing. The distributed magnetic force induced in the gap provides the actuation force $F_m$, which for a parallel gap is given by

$$F_m = \frac{1}{2}\frac{\Phi^2}{\mu_0 A} = \frac{1}{2}\frac{\mu_0 A (NI)^2}{d^2} \quad (\mu_r \rightarrow \infty), \qquad (9)$$

where $A$ is the area of the yoke at the location of the air gap, $d$ is the air-gap spacing, and $\mu_0$ is the permeability of free space. Note the analogy with the electrostatic force given by (1). The MMF $NI$ now replaces the electromotive force (EMF) $V$. Also here, due to the nonlinear dependence of $F_m$ on the distance $d$, instability occurs when the MMF exceeds the so-called pull-in MMF $NI_{PI}$. In lowering the current, after pull-in has occurred, the beam releases at a (much) lower MMF called the pull-out MMF $NI_{PO}$. As such, the electromagnetic actuator displays a hysteresis,

$$NI_{PI} = \sqrt{\frac{8}{27}\frac{kd_o^3}{\mu_0 A}} \quad (\mu_r \rightarrow \infty) \qquad (10a)$$

and

$$NI_{PO} = \sqrt{\frac{2k(d_o - d_R)d_R^2}{\mu_0 A}}, \qquad (10b)$$

where $d_o$ denotes the zero-flux gap spacing, k the effective spring stiffness of the beam, and $d_R$ the rest gap after closing. For a switch design for which $d_o = 2.5\ \mu$m, $d_R = 0.2\ \mu$m, $k = 10$ N/m, $A = 100 \times 100\ \mu\text{m}^2$, and $N = 100$ turns, it follows, that $I_{PI} \approx 0.6$ mA and $I_{PO} \approx 0.1$ mA. These are quite acceptable current levels, compared to rather high pull-in voltage obtained for a similar electrostatically

**The application of MEMS technology to RF/microwave systems is on the verge of revolutionizing wireless communications.**

actuated switch. It is pointed out that the magnetic force $F_m$ will not increase indefinitely with increasing current but is limited by flux saturation of the yoke material, $\Phi_{sat} = B_{sat} \cdot A_c$, where $A_c$ is the smallest cross-section in the flux path of the yoke. Saturation levels of magnetic induction $B_{sat}$ are typically in the range 0.5 to 1 T for ferromagnetic materials like permalloy ($Ni_{80}Fe_{20}$), leading to maximum forces in the range 1–4 mN for an area $A = A_c = 100 \times 100\ \mu\text{m}^2$, reached for current levels of 4–8 mA for a coil with $N = 100$ turns and an air gap of 1 $\mu$m. In other words, the maximum force achievable for the electromagnetic actuator, for acceptable current levels in the mA range, is three orders of magnitude higher than the achievable force for the electrostatic actuator for acceptable voltage levels below 10 V.

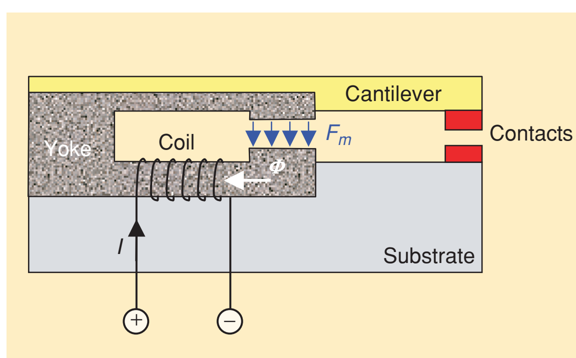


**Figure 8.** *Electromagnetic actuation mechanism illustrated on a microrelay.*

Another type of magnetic actuator exploits the Lorentz force acting on a current-carrying wire placed in an external magnetic field. This type of actuator is called an *electrodynamic* actuator, a name given by history to the voice coil-type actuator better known as a loudspeaker. The principle of operation of electrodynamic actuation is shown in Figure 9(a), and a specific implementation on a cantilever-type actuator is depicted in Figure 9(b). The Lorentz force $F_L$, acting on the current $I$ is given by

$$F_L = BIl, \qquad (11)$$

where $l$ is the section of the wire placed in the magnetic field. The above expression predicts a rather low Lorentz force of 0.1 $\mu$N acting on a wire that is 100 $\mu$m long, carries a current of 1 mA, and is placed in a magnetic field of 1 T. To achieve forces on the order 100 $\mu$N, as required for Au-Au contacts, a rather high current of 1 A is required. It is noteworthy that, contrary to electromagnetic actuation (as in Figure 8), instability does not occur for the electrodynamic actuator. Sensing of the beam motion relies on a change of the flux linkage of the current loop when the beam moves, thereby inducing an induction voltage, providing the detection signal [6].

As either electromagnetic or electrodynamic actuation, in essence, relies on current drive, the voltage can be quite low. This makes electromagnetic actuation attractive, as demonstrated by the few examples of electromagnetically driven microrelays [19], [20]. The drawbacks, however, are the continuous power consumption (current drain) when in the actuated state and the more complex fabrication technology (e.g., integrated coil, ferromagnetic materials). To alleviate the power consumption problem, magnetic latching, by using a permanent magnet, has been implemented in the relay developed by Magfusion [20]. This, however, is at the expense of a more complex fabrication technology and packaging technology.

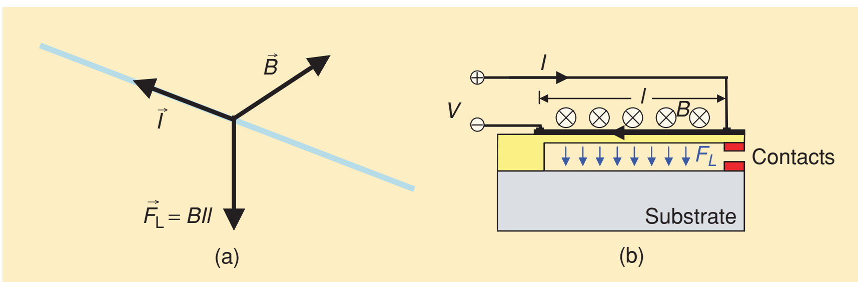


**Figure 9.** *Illustration of electrodynamic actuation. (a) Principle showing a current carrying wire placed in an magnetic field B, experiencing the Lorentz force $F_L$. (b) Implementation on a microrelay.*

## Packaging

MEMS devices, unlike ICs, contain movable fragile parts that must be packaged in a clean and stable environment. Encapsulation of the MEMS device is

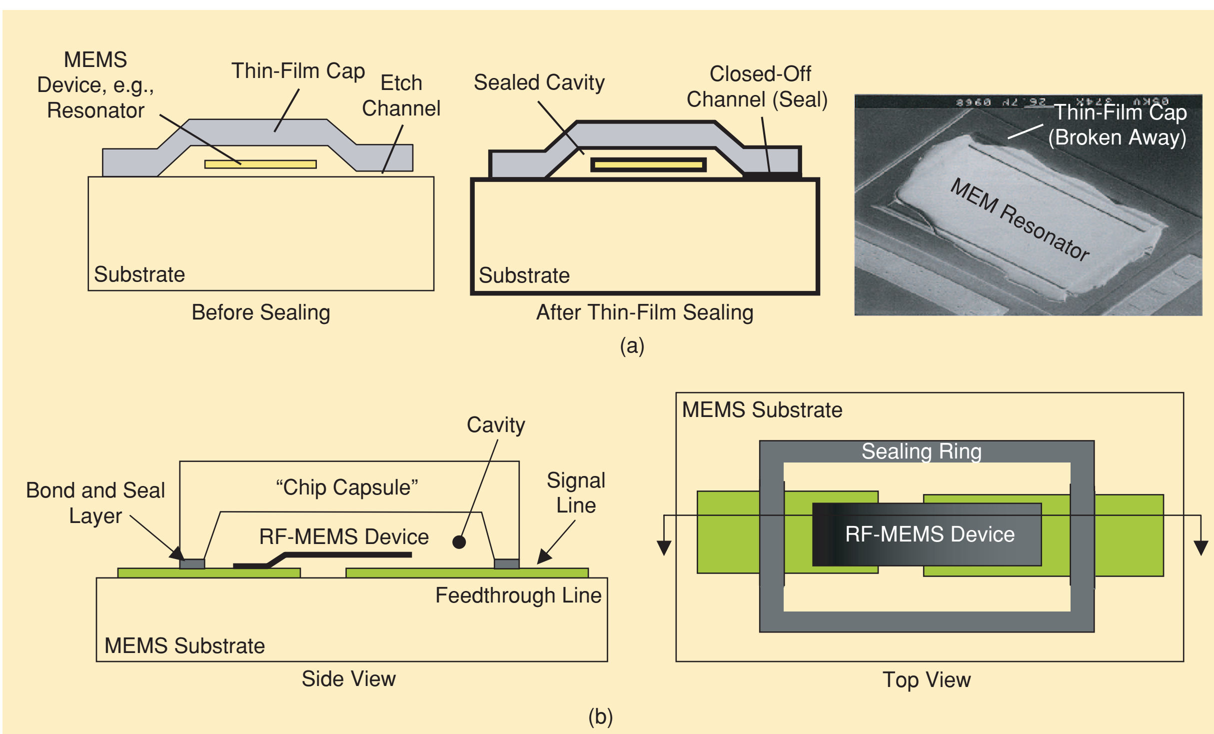


**Figure 10.** *Zero-level packaging: (a) using a thin film capsule; the SEM photo presents a sealed MEM resonator, shown after purposely removing the thin film capsule [23]. (b) using a bonded chip capsule.*

possible using hermetic one-level ceramic or metal-can packages, but the cost is high, and the technology is complex. For instance, standard wafer sawing cannot be used, as it will destroy the movable MEMS. This means that packaging must be preferably carried out during wafer processing, prior to die singulation. This packaging step is referred to as *zero-level packaging*, which creates an on-wafer device scale enclosure around (or sealed cavity for) the MEMS device, serving as a first protective interface. Two general approaches have been taken, here referred to as "thin-film capping" and "chip-capping," illustrated in Figure 10(a) and (b), respectively [21].

In either case, apart from low cost, the package has to satisfy certain application-specific technical requirements, including:

- protection against handling and harsh environments during assembly and operation
- screening/shielding against electrical, magnetic and electromagnetic (light) fields
- high (shear, pull, and hydrostatic) strength
- controlled-cavity ambient (pressure and gas composition)
- (near) hermetic cavity seal
- low-loss dc, RF, and microwave electrical feedthroughs
- minimal impact on device performance characteristics
- low-temperature process (e.g., $< 350\,^{\circ}$C)
- good heat-exchange (heat dissipation)
- minimal thermal stresses due to coefficient of thermal expansion (CTE) mismatch
- easy integration with front-end (MEMS) process.

**Thin-film capping relies on surface-micromachining and has been implemented in the past for various MEMS devices like pressure transducers [22], MEM resonators [23], and accelerometers [24].**

Thin-film capping relies on surface-micromachining and has been implemented in the past for various MEMS devices like pressure transducers [22], MEM resonators [23], and accelerometers [24]. In preparing the thin-film encapsulation, an access or etch channel in the cavity wall is foreseen [see Figure 10(a)]. The sacrificial layer etchant, e.g., a buffered HF solution if silicon oxide is used as the sacrificial layer, enters through this channel. After removal of the sacrificial layer, the etch channel is sealed off using, for instance, a conformal coating of low-pressure chemical vapor deposition (LPCVD) nitride [23], a plasma-enhanced chemical vapor deposition (PECVD) oxide layer [24], or a deposited

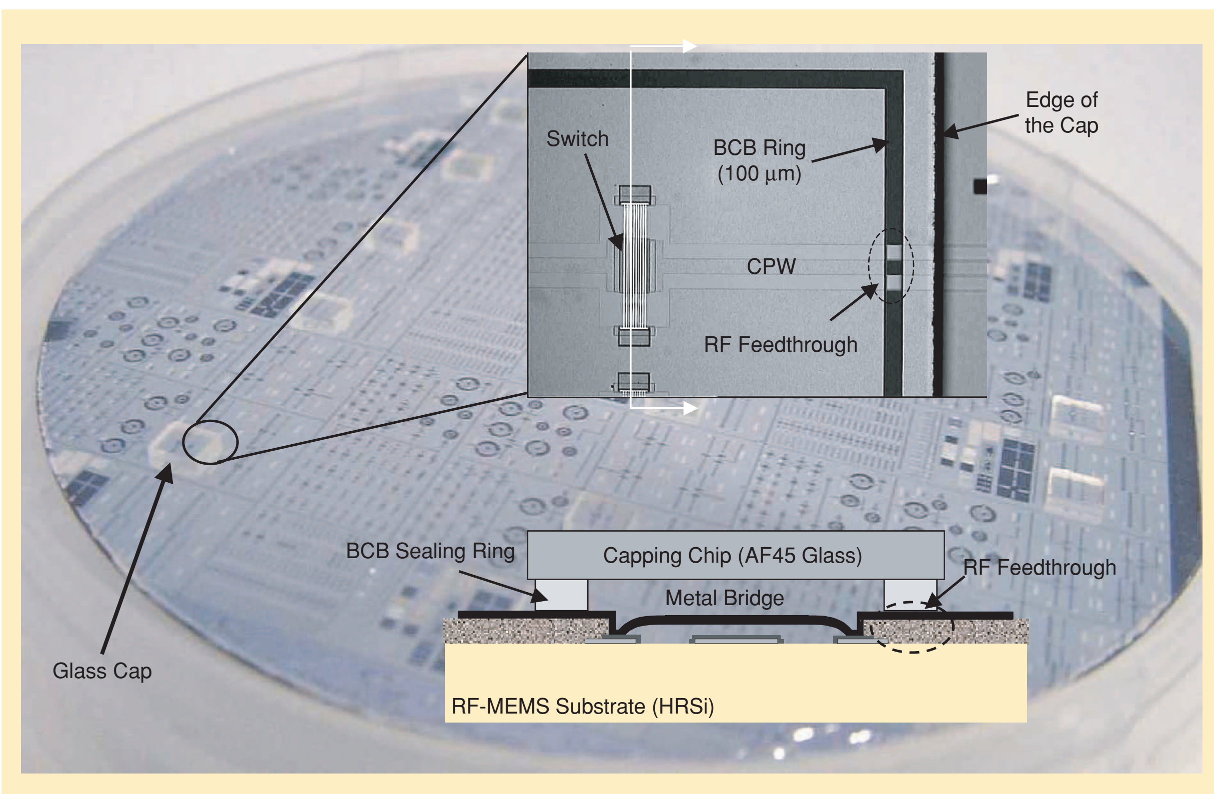


**Figure 11.** *Zero-level packaged RF-MEMS switches using BCB (cap-to-wafer assembly) [29].*

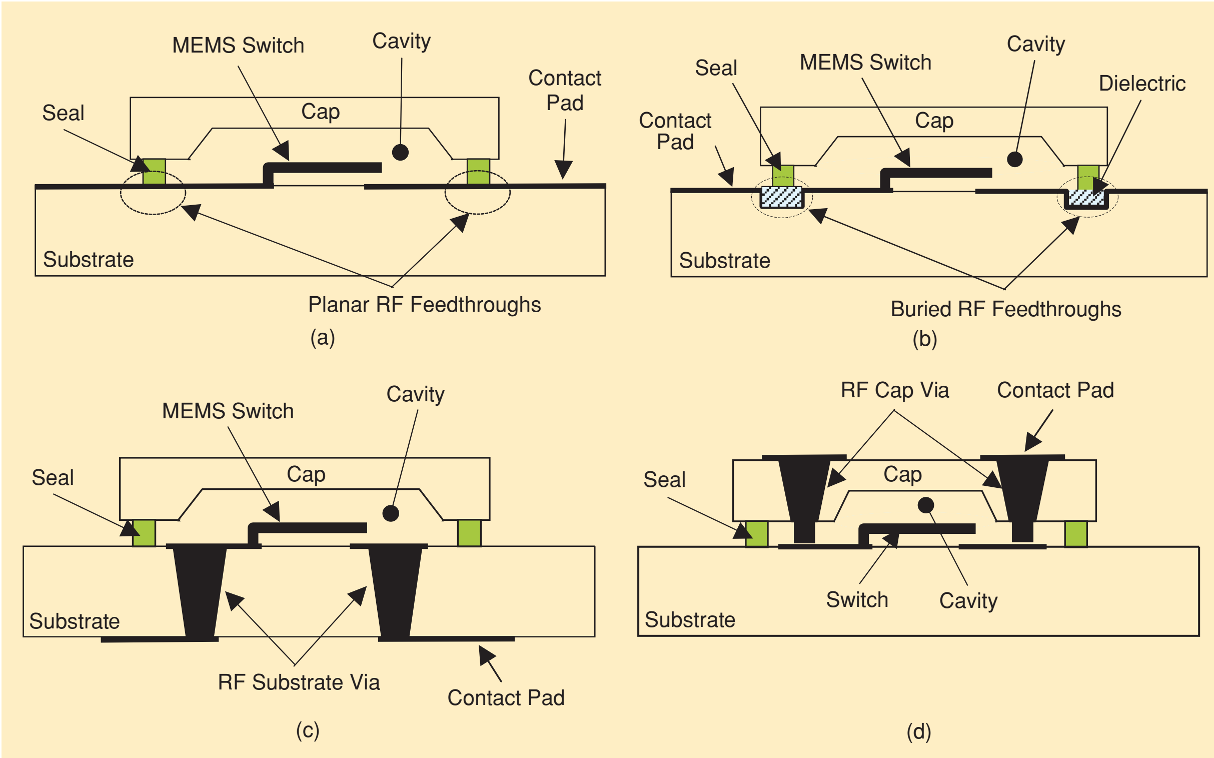


**Figure 12.** *Possible implementation of the RF transitions for a zero-level packaged RF-MEMS switch. (a) Horizontal planar RF feedthrough, (b) Horizontal buried RF feedthrough. (c) Substrate RF via. (d) Cap RF via.*

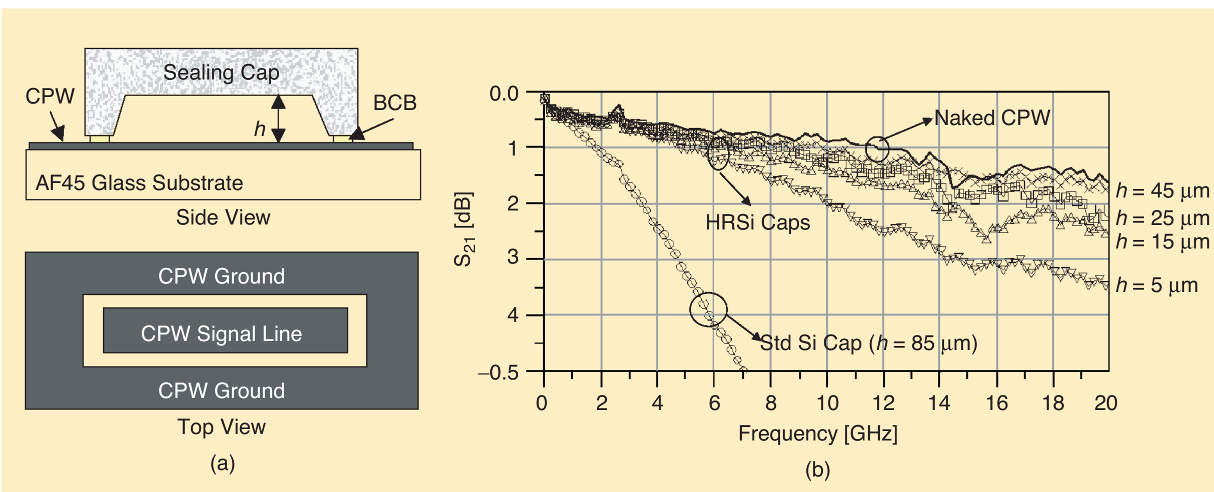


**Figure 13.** *Zero-level packaged CPW line (25/100/25 μm, 2.3 mm long, 3 μm thick Cu) implementing a horizontal coplanar feedthrough [34]. (a) Side and top view. (b) Measured $S_{21}$ on AF45 substrate capped with a LRSi cap (1–10 Ωcm, h=85 μm) and HRSi (>4,000 Ωcm) caps with varying cavity height.*

metal [25]. As of today, examples of thin-film capping for metal RF-MEMS switches or tunable capacitors do not exist in the open literature. In part, this is because metal RF MEMS built nowadays use aluminum or gold and, therefore, cannot be exposed to the high-temperatures ($>400$ °C) used for the deposition and sealing process of the thin-film cap. Furthermore, sealing at reduced pressure (e.g., as for an LPCVD nitride seal) is not desired as switches and tunable capacitors must operate at "standard" pressures in an inert ambient for reliable operation with no contact bouncing or long settling times (due to the absence of damping). From the viewpoint of temperature budget, metal thin-film encapsulation is a possibility, but the method described in [25] leads to a vacuum package.

Chip capping, on the other hand, has the advantage of a large flexibility in processing temperatures and control of the environment. In chip capping, it is common practice to bond a recessed capping chip onto the MEMS device wafer, as illustrated in Figure 10(b). The bonding and sealing ring is typically 50–300 $\mu$m in width. The bonding must be performed at sufficiently low temperatures (typically below 350 °C) such that the metallization and other materials of the RF-MEMS device are not adversely affected. Bonding techniques that can be used for this purpose include, solder bonding, gold-gold thermocompression bonding, and bonding using low temperature glasses ("frit" seals), epoxy seals, or polymer adhesives as the brazing material. The bond is characterized by its strength (shear and pull strength) and the hermeticity of the seal. Device performance can strongly depend on the ambient conditions. For instance, capillary forces, due to an absorbed liquid (moisture) film or any organic deposits and contaminants, can "glue" contacting surfaces together. Metals may corrode due to moisture inside the cavity. Also the *Q*-factor of MEM resonators is strongly dependent on the ambient pressure [23]. A reliable design, therefore, should entail a hermetic zero-level package that prevents moisture and other organic contaminants from migrating into the active region of the device. Most polymers suffer from serious moisture uptake. The best seals remain (impermeable) glass, silicon nitride, ceramics and metals. A very promising alternate method employs localized heating in which the heat dissipation is confined to a small region around the bond [26]. This allows rather high bonding temperatures (e.g., as high as 800 °C), potentially offering better and faster temperature control, improved bonding quality and broader choice of materials that can be bonded with likely better sealing properties than the low-temperature materials. Another important consideration for MEMS zero-level packages is the extremely small cavity volumes (hundreds of nanoliters). A stable pressure inside the cavity demands extremely low leak rates (better than $10^{-15}$ mbar.l/s [27]) and further makes that "outgassing" of atmospheric gases and packaging-material vapors from the surfaces of the cavity rapidly results in an significant change in pressure. The inclusion of getter materials, like Pd, Pt, Ti, or Zr-Al-Fe, inside RF-MEMS packages, used to absorb moisture and other gases, is considered as a viable solution for controlling the cavity ambient [28].

**The one-level package provides mechanical and environmental protection to the devices they hold but not without degrading the electrical performance.**

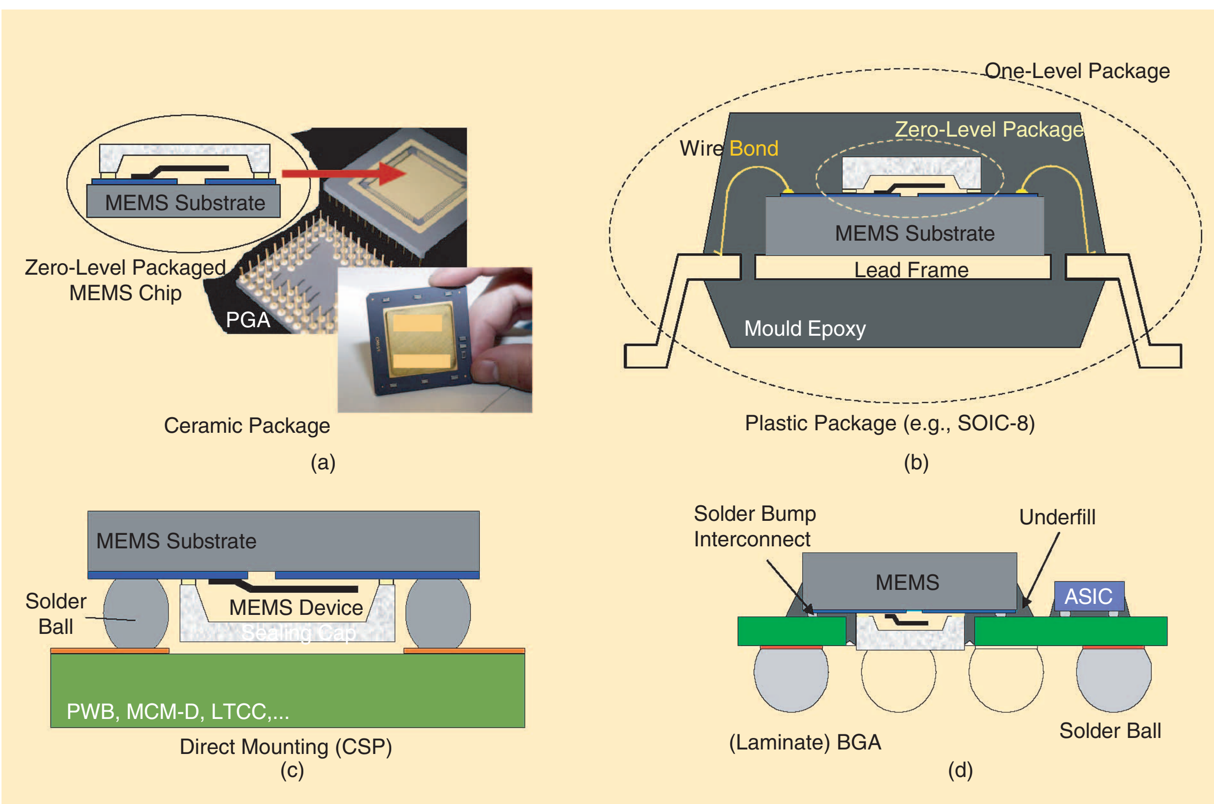


**Figure 14.** *Examples of one-level packaging of (RF-)MEMS devices.*

Since the start of RF-MEMS switch development, many research groups have neglected the packaging of these devices. Very often, the devices were developed independent of the package, until recently, when first publications on zero-level packaged RF-MEMS switches appeared [29]–[31]. For the zero-level package of the RF-MEMS switches developed at IMEC, chip capping using two different bonding methods are investigated. One relies on solder [19], [32], and the other on Benzocyclobutene (BCB) [27], [29] as the bonding and sealing layer. An example of a zero-level packaged capacitive RF-MEMS switch, developed in collaboration with Alcatel Microelectronics (now AMIS), is shown in Figure 11 [30]. BCB is used as the bonding and sealing material. BCB has excellent RF properties in addition to minimal outgassing and low moisture uptake. The sealing caps are made of low-loss borosilicate glass (AF45). Chip-on-wafer assembly using a flip-chip aligner and bonder was used to cap the individual switches. Strong bonds have been obtained, displaying shear strengths better than 10 MPa. Gross leaks (leak rate $>10^{-4}$ mbar.l/s) were not observed, meaning that the MEMS are well protected during handling and back-end processing (e.g., final wafer dicing). True hermeticity, on the other hand, cannot be expected from a polymer like BCB. First tests have indicated leak rates for BCB sealed cavities in the range $10^{-7}$–$10^{-8}$ mbar.l/s for ~100 $\mu$m wide sealing rings.

**The fact that RF MEMS enables superior passive devices, makes it a prime candidate to enable a plethora of wireless appliances operating in the home/ground, mobile, and space spheres.**

In packaging an RF-MEMS switch (or any other (RF-MEMS device), the package itself should have minimal effect on the device performance. In an ideal package, the RF characteristics, before and after capping, should be the same. This requires low-loss RF transitions and minimal induced loss and detuning of the transmission lines due to proximity coupling to the cap. Four possible implementations of RF transitions can be envisioned, as illustrated in Figure 12 [33]:

1) coplanar horizontal feedthroughs, see Figure 12(a) [29], [34]
2) buried horizontal feedthroughs, see Figure 12(b) [32]
3) vertical vias through the substrate, see Fig. 12(c) [30], [31]
4) vertical vias through the capping chip, see Figure 12(d).

The implementations using vertical vias present a more compact solution than the horizontal feedthrough designs, but the process is more complex, as through-wafer hole etching is required. In terms of RF performance, similar behavior is expected for all four implementations, noting that the buried feedthroughs require ever-narrower line widths at higher frequencies, e.g., above 30 GHz, resulting in an increased loss.

The coplanar horizontal feedthroughs, as implemented on the switches of Figure 11, are the simplest from a design and process point of view. The use of low-loss, high-resistivity cap materials and a cap with sufficient cavity height will largely suppress the degrading influence of the presence of the cap [34]. This is illustrated in Figure 13, showing an example of the RF performance of a coplanar feedthrough [as in Figure 12(a)] using BCB as the dielectric (and bond and seal layer) measured on a traversing coplanar waveguide (CPW) line. It is found that the impact on the RF characteristics of an RF-MEMS device built on a 50-Ω CPW line with ground-to-ground spacing of 150 $\mu$m, is kept negligibly small by using capping chips made of high-resistivity silicon and with a cavity height exceeding 45 $\mu$m, i.e., $\sim 1/3$ of the ground-to-ground spacing [34].

Once zero-level packaged, the MEMS product wafers can be handled like IC wafers and can be diced without great danger of breaking the MEMS device. After dicing, the zero-level-packaged devices are treated as individual die that can next be one-level packaged, e.g., mounted in a ceramic package [Figure 14(a)] or a plastic molded package [Figure 14(b)] [19], [30]. Alternatively, using more advanced packaging technologies, the assembly can be handled as a chip-scale package (CSP) and directly joint to a printed wiring board [Fig. 14(c)] or ball-grid array (BGA) laminate [Figure 14(d)].

The one-level package provides mechanical and environmental protection to the devices they hold but not without degrading the electrical performance. At microwave frequencies (and higher), the impact the package has on the electrical performance becomes an important element in the design of the device [35]. Plastic packaging [Figure 14(b)] is the most common packaging solution applicable for frequencies below several gigahertz. Careful choice of the plastic molding material and the RF design of the lead frame allows use up to 10 GHz. For use at higher frequencies, ceramic packages based on multilayer low-temperature cofired ceramic (LTCC) or high-temperature cofired ceramic (HTCC) technology, employing low-loss dielectrics combined with flip-chip assembly of the device for short interconnects, exhibit the potential for good performance into the millimeter-wave regime (as high as 80 GHz) [36].

## Conclusions

The fundamentals of RF-MEMS technology have been presented. In particular, the topics of fabrication (surface and bulk micromachining) techniques and their limitations, key physical actuation mechanisms upon which RF-MEMS devices may be predicated, and device-level packaging have been addressed.

Part two of this article follows and will deal with the progress and impact of three types of surface-micromachined RF-MEMS devices, namely, switchable capacitors (SC), varactors (variable/tunable capacitors), and ohmic switches on handsets, base stations, and satellites. In particular, issues such as system-level motivation/justification for RF MEMS, device requirements, high-volume manufacturing, packaging, and state-of-the-art performance and reliability, will be presented.

## References


[1] H.J. De Los Santos, *Introduction to Microelectromechanical (MEM) Microwave Systems.* Norwood, MA: Artech House, 1999.

[2] H.J. De Los Santos, "MEMS—A wireless vision," in *Proc. Int. MEMS Workshop*, Singapore, 2001, pp. 35–42.

[3] H.J. De Los Santos, *Introduction to Microelectromechanical (MEM) Microwave Systems*, 2nd ed. Norwood, MA: Artech House, 2004.

[4] T. Tsang, M. El-Gamal, S. Best, and H.J. De Los Santos, "Wide tuning range RF-MEMS varactors fabricated using the PolyMUMPs Foundry," *Microw. J.*, pp. 22–44, Aug. 2003.

[5] Th.G.S.M. Rijks, J.T.M. van Beek, P.G. Steeneken, M.J.E. Ulenaers, J. De Coster, and R. Puers, "RF MEMS tunable capacitors with large tuning ratio," in *Proc. MEMS 2004 Dig*, 2004, pp. 777–780.

[6] H.A.C. Tilmans and S. Bouwstra, "Excitation and detection of silicon-based micromechanical resonators," *Sens. Mater.*, vol. 9, pp. 521–540, Aug. 1997.

[7] J.J. Yao, "Topical review: RF MEMS from a device perspective," *J. Micromech. Microeng.*, vol. 10, no. 4, pp. R9–R38, Dec. 2000.

[8] G.M. Rebeiz, *RF-MEMS Theory, Design, and Technology*. New York: Wiley, 2003.

[9] S. Pamidighantam, R. Puers, K. Baert, and H.A.C. Tilmans, "Pull-in voltage analysis of electrostatically actuated beam structures with fixed-fixed and fixed-free end conditions," *J. Micromech. Microeng.*, vol. 12, pp. 458–464, 2002.

[10] A.P. DeSilva, C. Vaughan, D. Frear, L. Liu, S.M. Kuo, J. Foerstner, J. Drye, J. Abrokwah, H. Hughes, C. Amrine, C. Butler, S. Markgraf, H. Denton, and S. Springer, "Motorola MEMS switch technology for high frequency applications," in *Proc. MEMS Conf.*, Berkeley, CA, 2001, pp. 22–24.

[11] T. Ikeda, *Fundamentals of Piezoelectricity*, New York: Oxford Univ. Press, 1989.

[12] J.G. Smits and W. Choi, "The constituent equations of piezoelectric heterogenous bimorphs," *IEEE Trans. Ultrason., Ferroelect. Freq. Contr.*, vol. 38, no. 3, pp. 256–270, 1991.

[13] S.J. Gross, S. Tadigadapa, T.N. Jackson, S. Trolier-McKinstry, and Q.Q. Zhang, "Lead-zirconate-titanate-based piezoelectric micromachined switch," *Appl. Physi. Lett.*, vol. 83, no. 1, pp. 174–176, July 2003.

[14] J.Y. Park, Y.J. Yee, H.J. Nam, and J.U. Bu, "Micromachined RF MEMS tunable capacitors using piezoelectric actuators," in *Proc. IEEE MTT-S,* Phoenix, AZ, 2001, pp. 2111–2114.

[15] G. Piazza, R. Abdolvand, G.K. Ho, and F. Ayazi, "Voltage-tunable piezoelectrically-transduced single-crystal silicon micromechanical resonators," *Sens. Actuators A, Phys.*, vol. 111, pp. 71–78, no. 1, 2004.

[16] R.J. Wilfinger, P.H. Bardell, and D.S. Chhabra, "The resonistor: A frequency selective device utilizing the mechanical resonance of a silicon substrate," *IBM J. Res. Develop.*, vol. 12, pp. 113–118, 1968.

[17] T.S.J. Lammerink, M. Elwenspoek, R.H. van Ouwerkerk, S. Bouwstra, and J.H.J. Fluitman, "Performance of thermally excited resonators," *Sens. Actuators*, vol. A21–A23, no. 1–3, pp. 352–356, 1990.

[18] D. Saias, P. Robert, S. Boret, C. Billard, G. Bouche, D. Belot, and P. Ancey, "An above IC MEMS RF switch," *IEEE J. Solid-State Circuits*, vol. 38, pp. 2318–2324, Dec. 2003.

[19] H.A.C. Tilmans, E. Fullin, H. Ziad, M. Van de Peer, J. Kesters, E. Van Geffen, J. Bergqvist, M. Pantus, E. Beyne, K. Baert, and F. Naso, "A fully-packaged electromagnetic microrelay," in *Proc. MEMS '99,* Orlando, FL., pp. 25–30.

[20] M. Ruan, J. Shen, and C.B. Wheeler, "Latching micromagnetic relays," *J. MEMS*, vol. 10, no. 4, pp. 511–517, 2001.

[21] K. Najafi, "Micropackaging technologies for integrated microsystems: Applications to MEMS and MOEMS," *Proc. SPIE*, vol. 4979, pp. 1–19, 2003.

[22] H. Guckel and D.W. Burns, "A technology for integrated transducers," in *Proc. Transducers'85*, Philadelphia, PA, pp. 90–92.

[23] R. Legtenberg and H.A.C. Tilmans, "Electrostatically driven vacuum encapsulated polysilicon resonators, Part I: Design and fabrication," *Sens. Actuators A, Phys.*, vol. 45, no. 1, pp. 57–66, 1994.

[24] H. Stahl, A. Hoechst, F. Fischer, L. Metzger, R. Reichenbach, F. Laermer, S. Kronmueller, K. Breitschwerdt, R. Gunn, R. Watcham, C. Rusu, and A. Witvrouw, "Thin film encapsulation of acceleration sensors using polysilicon sacrificial layers," in *Proc. Transducers'03,* Boston, MA, pp. 1899–1902.

[25] B.H. Stark and K. Najafi, "An ultra-thin hermetic package utilizing electroplated gold," in *Proc. Transducers'01,* Munich, Germany, pp. 194–197.

[26] L. Lin, "MEMS post-packaging by localized heating," *IEEE Trans. Adv. Pack.*, vol. 23, no. 4, pp. 608–616, 2000.

[27] A. Jourdain, P. De Moor, S. Pamidighantam, and H.A.C. Tilmans, "Investigation of the hermeticity of BCB-sealed cavities for housing (RF-)MEMS devices," in *Proc. MEMS 2002,* Las Vegas, NV, pp. 677–680.

[28] K. Gilleo and S. Corbett, "Getters-molecular scavengers for packaging," *HDI*, pp. 26–29, Jan. 2001.

[29] H.A.C. Tilmans, H. Ziad, H. Jansen, O. Di Monaco, A. Jourdain, W. De Raedt, X. Rottenberg, E. De Backer, A. De Caussemaeker, and K. Baert, "Wafer-level packaged RF-MEMS switches fabricated in a CMOS fab," in *Proc. IEDM 2001,* Washington, DC, pp. 921–924.

[30] M. Fujii, I. Kimura, T. Satoh, and K. Imanaka, "RF MEMS switch with wafer level package utilizing frit glass bonding," in *Proc. 32nd European Microwave Conf.*, Milan, Italy, 2002, vol. 1, pp. 279–281.

[31] A. Margomenos, D. Peroulis, K.J. Herrick, and L.P.B. Katehi, "Silicon micromachined packages for RF MEMS switches," in *Proc. 31st European Microwave Conf.*, London, UK, 2001, vol. 1, pp. 271–274.

[32] A. Jourdain, S. Brebels, W. De Raedt, and H.A.C. Tilmans, "The influence of 0-level packaging on the performance of RF-MEMS devices," in *Proc. 31st European Microwave Conf.*, London, UK, 2001, vol. 419, pp. 403–406.

[33] H.A.C. Tilmans, "MEMS components for wireless communications," [CD-ROM] in *Proc. EUROSENSORS XVI*, Prague, Czech Republic, 2002, pp. 1–34.

[34] A. Jourdain, X. Rottenberg, G. Carchon, and H.A.C. Tilmans, "Optimization of 0-level packaging for RF MEMS devices," in *Proc. Transducers'03*, Boston, MA, pp. 1915–1918.

[35] A. Chandrasekhar, S. Brebels, S. Stoukatch, E. Beyne, W. De Raedt, and B. Nauwelaers, "The influence of packaging materials on RF performance," *Microelectronics Reliability*, vol. 43, no. 3, pp. 351–357, 2003.

[36] M. Ito, K. Maruhashi, N. Senba, N. Takahashi, and K. Ohata, "Low cost multi-layer ceramic package for flip-chip MMIC up to W-band," in *2000 IEEE MTT-S Dig.*, 2000, pp. 57–60.